

Disorder-Induced Microscopic Magnetic Memory

M. S. Pierce,¹ C. R. Buechler,¹ L. B. Sorensen,¹ J. J. Turner,² S. D. Kevan,² E. A. Jagla,³ J. M. Deutsch,⁴ T. Mai,⁴ O. Narayan,⁴ J. E. Davies,⁵ K. Liu,⁵ J. Hunter Dunn,⁶ K. M. Chesnel,⁷ J. B. Kortright,⁷ O. Hellwig,^{8,*} and E. E. Fullerton.⁸

¹*Department of Physics, University of Washington, Seattle, Washington 98195, USA*

²*Department of Physics, University of Oregon, Eugene, Oregon 97403, USA*

³*The Abdus Salam International Centre for Theoretical Physics, Trieste, Italy*

⁴*Department of Physics, University of California, Santa Cruz, California 95064, USA*

⁵*Department of Physics, University of California, Davis, California 95616, USA*

⁶*MAX Laboratory, Box 118, SE-221 00 Lund, Sweden*

⁷*Lawrence Berkeley National Laboratory, Berkeley, California 94720, USA*

⁸*Hitachi Global Storage Technologies, San Jose, California 95120, USA*

(Received 10 November 2003; published 6 January 2005)

Using coherent x-ray speckle metrology, we have measured the influence of disorder on major loop return point memory (RPM) and complementary point memory (CPM) for a series of perpendicular anisotropy Co/Pt multilayer films. In the low disorder limit, the domain structures show no memory with field cycling—no RPM and no CPM. With increasing disorder, we observe the onset and the saturation of both the RPM and the CPM. These results provide the first direct ensemble-sensitive experimental study of the effects of varying disorder on microscopic magnetic memory and are compared against the predictions of existing theories.

DOI: 10.1103/PhysRevLett.94.017202

PACS numbers: 75.60.Ej, 07.85.Qe, 61.10.-i, 78.70.Dm

The magnetic recording industry deliberately introduces carefully controlled disorder into its materials to obtain the desired hysteretic behavior. Over the past 40 years, such magnetic hardening has developed into a high art form [1]. Although we do not yet have a satisfactory *fundamental microscopic* description of magnetic hysteresis, beautiful theories of magnetic memory based on random microscopic disorder have been developed over the past ten years [2]. How well do these theories compare with experimental results? To address this question, we have deliberately introduced increasing degrees of disorder into a series of thin multilayer perpendicular magnetic materials and studied how the configuration of the magnetic domains evolve as these systems are cycled around their major hysteresis loops.

Until very recently [3], our best information about the repeatability of the domain configurations was deduced from the associated magnetic avalanches via the Barkhausen noise [4]. Our best current microscopic theories [2] were built on the microscopic information provided by Barkhausen measurements and on the macroscopic information provided by classical magnetometry measurements. If the Barkhausen noise repeats perfectly for every cycle of the major loop, then the avalanches occur in precisely the same time order and it is plausible to infer that the microscopic spatial evolution of the domains is also the same. However, very recently it became possible to directly probe the precise spatial distribution of the magnetic domains using coherent x-ray speckle metrology (CXSM) instead of indirectly inferring the domain configurations from the time sequence of the avalanches [3].

Here we have applied this powerful new CXSM technique to investigate the effects of disorder on the domain

evolution in a series of Co/Pt multilayer samples with perpendicular magnetic anisotropy. In addition to their possibly profound implications for the existing theories about the disorder and avalanches in 2D systems [2], such perpendicular magnetic films are of intense current interest because they promise significant increases in magnetic storage density [1].

We address two long-standing questions in this Letter: (1) The existence of quasistatic major hysteresis loops naturally raises the first question: how is the microscopic magnetic domain configuration at one point on the major loop related to the configurations at the same point on the major loop during subsequent cycles? We will call this effect major loop microscopic return point memory (RPM). There are two limiting possibilities for this evolution: (a) the domains evolve in precisely the same deterministic way during each cycle; this is the prediction of all of the best current (zero-temperature) microscopic theories [2]. (b) The domains evolve completely differently during each cycle; their evolution is completely nondeterministic; this is the expectation for thermally dominated systems. There has been surprisingly little theoretical work on nonzero-temperature models. We show below that our samples exhibit behavior intermediate between these two limits—their memories improve with increasing disorder, yet never become perfect. (2) The inversion symmetry of the quasistatic major hysteresis loops through the origin naturally raises the second question: how are the magnetic domains at one point on the major loop related to the domains at the complementary point during the same and during subsequent cycles? We will call this effect major loop complementary point memory (CPM) [5].

Our samples were grown by magnetron sputtering on silicon-nitride-coated, smooth, low-stress 1 cm by 1 cm silicon wafers. Each wafer had a 2 mm by 2 mm square 160-nm-thick freestanding SiN_x membrane at its center. We used this thin SiN_x window for our transmission CXSM measurements. Our samples all had $[\text{Co}(0.4 \text{ nm})/\text{Pt}(0.7 \text{ nm})]_{50}$ with Pt buffer layers (20 nm) and Pt caps (2.3 nm). Our sample numbers correspond to the pressure (in milliTorr) of the argon gas that we used to sputter them. For low argon pressures, the sputtered metal atoms arrive at the substrate with considerable kinetic energy which locally heats and anneals the growing film, leading to smooth Co/Pt interfaces [6]. For higher argon sputtering pressures, the sputtered atoms arrive at the growth substrate with minimal kinetic energy, resulting in rougher Co/Pt interfaces [6].

We measured the major hysteresis loops for all of our samples using both Kerr and SQUID magnetometry. The properties of the major loops show clear changes that are related to the increasing roughness. Figure 1 shows that the shape of the major loops change from being nucleation-dominated to being disorder-dominated. Table I shows that the saturation magnetization decreases as the microscopic disorder increases. Our smoother samples (3 and 7) exhibit soft loops with low remanence and distinct domain nucleation. Between 7 and 8.5, there is a transition to loops which do not show a distinct domain nucleation region. Between 8.5 and 20, the ascending and descending slopes of each loop remain the same, but the loops gradually widen until the full magnetic moment is left at remanence. We show below that this change in character of the loops coincides with the change in their measured RPM and CPM.

In addition, we also found via magnetometry that all of our films exhibit *perfect macroscopic major and minor loop* RPM and CPM [3]. This shows that the ensemble-average magnetization is the same for any given point on a loop, but it does not prove that the individual magnetic

domains are precisely the same. We show below, in fact, that even for our hard magnetic films with essentially complete remanence, that less than $\sim 60\%$ of the domains are identical after reversal.

Our experiments were performed at the Advanced Light Source at Lawrence Berkeley National Laboratory. We used linearly polarized x rays from the third and higher harmonics of the beam line 9 undulator. The photon energy was set to the cobalt L_3 resonance at ~ 778 eV. To achieve transverse coherence, the raw undulator beam was passed through a 35-micron-diameter pinhole before being scattered in transmission by the sample. The resonant magnetic scattering was collected by a soft x-ray charge-coupled device camera. The magnetization of the film was varied by an electromagnet, which applied fields perpendicular to the film.

The effects of our controlled disorder on the magnetic domains in real space and reciprocal space are shown in Fig. 2. The magnetic force microscopy (MFM) images on the top show that the domains form characteristic wormlike labyrinths at low disorder but that these labyrinths become increasingly indistinct as the structural disorder is increased. The magnetically scattered intensities versus the radial wave vector transfer are shown on the bottom. They show (1) that the magnetic correlation length decreases with increasing disorder, (2) that the magnetic domain size distribution is well defined even though it is not visible in the MFM images, and (3) that increasing the disorder decreases the characteristic domain size.

We have previously shown that changes in the magnetic domain structure can be measured via their magnetic speckle patterns [3]. To quantify the correlation between two speckle patterns, we use image auto and cross correlation to extract the generalized correlation coefficient ρ , which is unity when the speckle patterns are identical and is zero when the speckle patterns are completely uncorrelated [3].

The first question that we addressed was whether our samples exhibited major loop microscopic RPM. To do so, we compared two speckle patterns collected at the same point on the major loop, but separated by one or more full excursions around the major loop. For our smooth samples

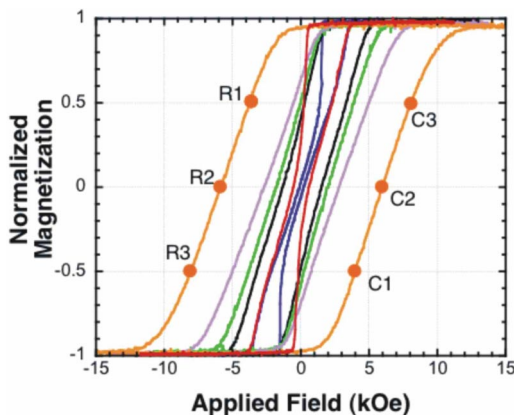


FIG. 1 (color online). Measured magnetic hysteresis loops. Starting at the origin, and moving to increasing applied field $|H|$, the loops shown are for samples 3, 7, 8.5, 10, 12, and 20. The inversion symmetry through the origin is shown.

TABLE I. Co/Pt Sample Characteristics.

| Sample ^a | σ_{rms} ^b | M_s ^c | H_c ^d |
|---------------------|------------------------------------|--------------------|--------------------|
| 3 | 0.48 | 1.36 ± 0.06 | 0.08 ± 0.01 |
| 8.5 | 0.62 | 1.14 ± 0.05 | 1.3 ± 0.2 |
| 10 | 0.69 | 1.07 ± 0.05 | 1.6 ± 0.2 |
| 12 | 0.90 | 1.10 ± 0.05 | 2.5 ± 0.3 |
| 20 | 1.44 | 0.92 ± 0.04 | 5.9 ± 0.2 |

^aGrowth pressure, milliTorr.

^brms interfacial roughness, nm.

^cSaturation magnetization of Co, 10^3 emu/cm³.

^dCoercive field, kOe.

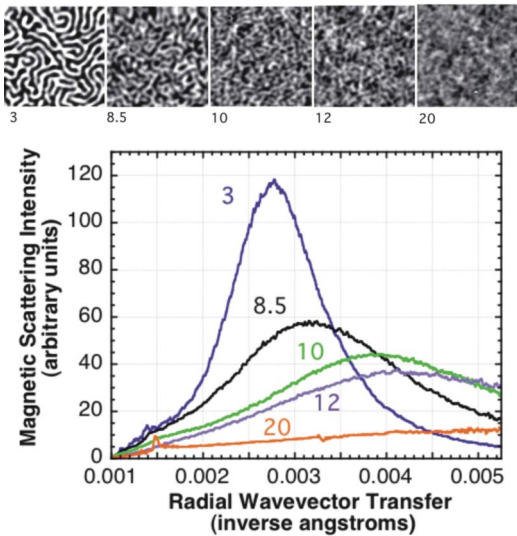


FIG. 2 (color online). Measured effects of the argon sputtering pressure on the magnetic domains. Top: real space. Three square micron MFM images of the magnetic domain structure at remanence are shown. Note the apparent disappearance of the labyrinthine structure as the disorder grows. Bottom: reciprocal space. The radial profiles measured by coherent x-ray magnetic scattering at the coercive point. The labels (3, 8.5, 10, 12, and 20) indicate the argon sputtering pressure in milliTor during the growth of that film (see Table I).

with soft loops, we found little correlation between these speckle patterns. In sharp contrast, we always found strong correlations peaking near $\rho \sim 0.6$, for our rougher, hard-loop samples.

The second question that we addressed was if our samples exhibited major loop microscopic CPM. To do so, we compared the speckle pattern collected at one point on the major loop with speckle patterns collected at the inversion-symmetric complementary point on subsequent cycles. Again, for our lowest disorder samples, we found no correlation between these speckle patterns—zero CPM values. However, for the more disordered samples, we found significant, nonzero CPM values that were consistently smaller than the corresponding RPM values.

Our measured RPM and CPM values for sample 8.5 are shown in Fig. 3. The data for three sequential complete excursions around the major loop are shown. For each value of the applied field H , Fig. 3 shows the measured RPM and CPM values for that field. There are several interesting trends: (1) Neither the RPM value nor the CPM value depends on the number of intermediate loops or on the choice of the starting half loop. This indicates that the deterministic components of the RPM and CPM are essentially stationary. This implies that the memory in our system is largely reset by bringing the sample to saturation. It also strongly suggests that the same disorder is producing both the RPM and the CPM. (2) Our RPM values are consistently larger than our CPM values. (3) Both the RPM and the CPM values are largest near the initial domain

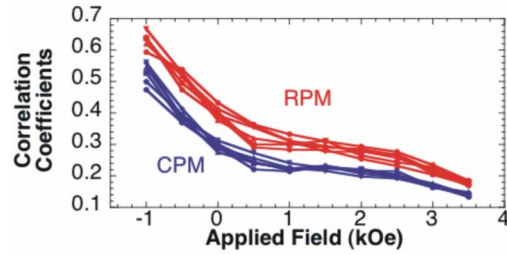


FIG. 3 (color online). Measured RPM and CPM values versus the applied field for the 8.5 milliTor sample.

nucleation region, which occurs at about -1 kOe for this sample. This suggests that the subsequent decorrelation is produced by the domain growth; this is confirmed by our magnetic x-ray imaging studies. (4) Both the RPM and the CPM values decrease monotonically to their minimum values near complete reversal which occurs at about 4 kOe for this sample. This again suggests that the decorrelation is produced by the domain growth.

Figure 4 shows our major loop microscopic RPM and CPM correlation coefficients, measured at the coercive point for each sample, plotted versus our measured rms roughness. We measured the interfacial roughness for each sample by taking multiple atomic force microscope (AFM) images and calculating the rms variation of the measured heights. We also verified that the roughness in our samples was conformal and increased monotonically with the argon sputtering pressure by measuring their specular x-ray reflectivities using 0.154 nm x rays. As noted above, our two smooth samples have essentially zero RPM and CPM values. In contrast, all of our rough samples exhibit nonzero RPM and CPM values that increase as the roughness

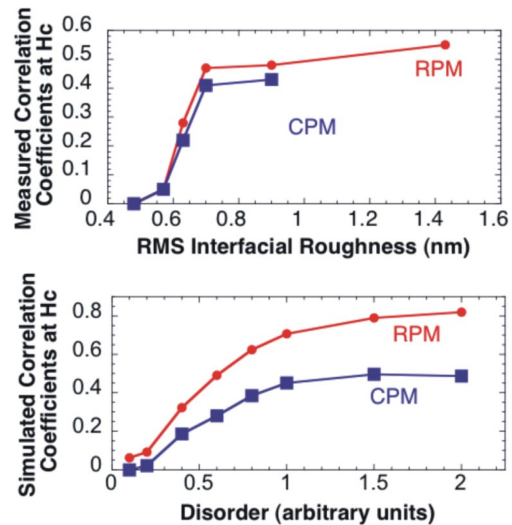


FIG. 4 (color online). RPM and CPM values at the coercive point versus disorder. Top: our measured RPM and CPM values versus the measured rms roughness. Bottom: the RPM and CPM values obtained from our nonzero-temperature numerical simulations that combine the RCIM and the RFIM.

increases. This increase starts precisely where the major loops change from being nucleation-dominated to being disorder-dominated.

Our results are the first direct measurements of the effects of controlled microscopic disorder on microscopic return point memory and complementary point memory for major loops. How can we understand our experimental results in the light of the current microscopic disorder theories, and, in particular, the discrepancy between the RPM and CPM values?

A widespread approach in the literature is to approximate the spins as Ising, to use simple spin-flip dynamics, which is controlled solely by the energy of each spin, and to consider zero temperature. It is easy to see then, that for models where the energy is unchanged when all the spins (and the external field) are reversed, that the configurations that the system goes through on the ascending and descending branches of the major hysteresis loop are precisely mirror images of each other, so that (at $T = 0$) the RPM and CPM values are both precisely unity. This is the standard prediction for the $T = 0$ random anisotropy, bond, and coercivity Ising models (RAIM, RBIM, RCIM). On the other hand, for the $T = 0$ random field Ising model (RFIM), only perfect RPM is predicted. Note that both of these predictions are contrary to our experimental results; it is therefore clearly important to include thermal effects in our simulations.

Within the Ising approximation with simple spin-flip dynamics at nonzero temperature, our experimental result (that the CPM value is comparable but always smaller than the RPM value) implies that the disorder has a small component that breaks spin-reversal symmetry. This can be modeled by combining (for example) the RFIM and the RCIM. Then our simulations using a dipolar ϕ^4 model [7] show that a random field with an amplitude of only $\sim 4\%$ of the spin-spin coupling can produce an effect similar to what we see experimentally. Our simulated results using this approximation are shown in Fig. 4. Physically, the necessary local random fields could come either from frozen impurity magnetic moments or from a very wide distribution of domain coercivities and incomplete saturation.

However, there is another potential origin for our observed RPM-CPM asymmetry. Even if the energy is spin-inversion-symmetric, the dynamics governing the spin reversal are not required to be. Our simulations of a spin-reversal-symmetric, disordered vector-spin model with strong Ising-like (locally varying) anisotropy, with the dynamics given by the standard Landau-Lifshitz-Gilbert-Bloch-Bloembergen formalism, show dynamic symmetry breaking [8]. Note that then the time evolution of any spin is given by a precessional term, which is unchanged under spin (and field) reversal, and by a relaxational term, which

is reversed. Therefore, the overall time evolution is not invariant under spin reversal, and the ascending and descending microscopic states along the major hysteresis loop are not the same.

Our results have very strong implications. Within the widely used approximation of Ising spins and simple spin-flip dynamics, they rule out all of the commonly used simple models—e.g., the RAIM, RBIM, RCIM and RFIM—and they necessitate a nonzero temperature combination of these. And if one goes beyond the simple Ising approximation, we have found that it is possible for the dynamics to break the spin-inversion symmetry even if the Hamiltonian is symmetric.

Our results show that there are still a variety of new interesting experimental and theoretical questions in this classic mature subject: what breaks the RPM-CPM symmetry? Can the different random Ising models be distinguished via the field dependence of the RPM and CPM values? It will be extremely interesting to see how the RPM and CPM values vary with the sample disorder and with sample temperature—particularly for technologically important magnetic memory materials.

We gratefully acknowledge support by the U.S. DOE via DE-FG02-04ER46102, DE-FG03-99ER45776, DE-AC03-76SF00098, and DE-FG06-86ER45275 and via LLNL-UCDRD. We also gratefully acknowledge helpful discussions with K. A. Dahmen and J. P. Sethna.

*Partially supported by the Deutsche Forschungsgemeinschaft via HE 3286/1-1 and is currently at BESSY GmbH, Berlin, Germany.

- [1] A. Moser *et al.*, J. Phys. D **35**, R157 (2002); K. Ouchi, IEEE Trans. Magn. **37**, 1217 (2001).
- [2] For RAIM, see E. Vives and A. Planes, Phys. Rev. B **63**, 134431 (2001); for RBIM, see E. Vives and A. Planes, J. Magn. Magn. Mater. **221**, 164 (2000); for RCIM, see O. Hovorka and G. Friedman, cond-mat/0306300; for RFIM, see J. P. Sethna, K. A. Dahmen, and O. Perkovic, cond-mat/0406320.
- [3] M. S. Pierce *et al.*, Phys. Rev. Lett. **90**, 175502 (2003); B. Hu *et al.*, Synchrotron Radiation News **14**, 11 (2001).
- [4] S. Zapperi and G. Durin, Comput. Mater. Sci. **20**, 436 (2001); J. R. Petta, M. B. Weissman, and G. Durin, Phys. Rev. E **57**, 6363 (1998); D. Spasojevic *et al.*, Phys. Rev. E **54**, 2531 (1996).
- [5] J. R. Hoinville *et al.*, IEEE Trans. Magn. **28**, 3398 (1992); A. Jander *et al.*, IEEE Trans. Magn. **34**, 1657 (1998); P. Fischer *et al.*, J. Phys. D **35**, 2391 (2002).
- [6] E. E. Fullerton *et al.*, Phys. Rev. B **48**, 17432 (1993).
- [7] E. A. Jagla, Phys. Rev. E **70**, 046204 (2004).
- [8] J. M. Deutsch, T. Mai, and O. Narayan, cond-mat/0408158.